



Toward a stress-based topology optimization procedure with indirect calculation of internal finite element information



Seung Hyun Jeong^a, Seon Ho Park^a, Dong-Hoon Choi^b, Gil Ho Yoon^{b,*}

^a Graduate School of Mechanical Engineering, Hanyang University, Republic of Korea

^b School of Mechanical Engineering, Hanyang University, Seoul, Republic of Korea

ARTICLE INFO

Article history:

Received 7 September 2012

Received in revised form 14 May 2013

Accepted 4 July 2013

Keywords:

Stress-based topology optimization

Finite element software package

Sensitivity analysis

ABSTRACT

In this work, a novel computational approach is developed for the gradient-based stress-based topology optimization method, where the volume is minimized according to locally defined stress constraints of static failure criteria in the framework of tailored finite element (FE) software without direct access to an internal finite element information database. Tailored finite element codes that require substantial understanding and modification (reprogramming) or do not directly provide internal finite element information have rarely been used for stress-based topology optimization with solid isotropic material with penalization (SIMP) methods. Therefore, much research has been confined to two-dimensional problems with rectilinear basic finite elements, as complex three-dimensional geometries with advanced finite element formulations are not supported. To overcome this problem, we developed a new computational procedure for sensitivity analysis without direct access to an internal information database, a task that has previously been regarded as almost impossible. Since the calculation of linear strain–displacement matrices is required in the sensitivity analysis, the present procedure includes a node selection algorithm to efficiently calculate the matrices of irregular-shaped finite elements by displacement perturbations. The benefits of the present approach are that well-established powerful finite element codes, i.e., commercial or sophisticated public FE codes, can be easily incorporated for linear stress-based topology optimization, and any type of finite element formulation can be readily employed. In contrast to classical sensitivity analysis, small computations are used for sensitivity analysis in this work. To demonstrate the validity and efficiency of the present procedure and approach, several topology optimization problems with 3D and shell elements are solved.

© 2013 Elsevier Ltd. All rights reserved.

1. Introduction

In this work, specific issues related to stress-based topology optimization are addressed in the framework of tailored finite element (FE) software packages, i.e. commercial FE or sophisticated open source FE codes not developed or modified for topology optimization. As it is important to determine the optimal layouts of linear structures while considering localized stress limits to prevent static or dynamic (fatigue) failures, there has been increasing interest in size optimization, shape optimization, and topology optimization for mechanical stress over the last few decades. To rigorously consider localized stress limits and the associated constraints in topology optimization, many theoretical and practical issues of the singular behavior of stress with respect to density design variables [1–12], the highly nonlinear behavior of stress constraints [6,10],

* Corresponding author. Tel.: +82 222200451.

E-mail addresses: gilho.yoon@gmail.com, ghy@hanyang.ac.kr (G.H. Yoon).

and the compromise between local and global stress constraints [6,7,9–11] have been studied. In addition, since sensitivity analyses of local and global stress constraints require internal FE information (e.g., the stress, strain, element stiffness, and strain–displacement matrix), the internal database of tailored FE software should be accessible. However, such accessibility is normally difficult or not allowed. Consequently, it seems that most topology optimization research regarding mechanical stress has employed specialized in-house FE codes that operate in limited two-dimensional computational domains, which do not represent real engineering structures. Therefore, we propose a new computational approach to implement the sensitivity analysis of topology optimization problems in tailored finite element programs without modification of the programs [13–16].

In this research, the above biased trend regarding stress constraints is overcome through the development of a new computational procedure. In this scheme, blinded FE information required for stress topology optimization is computed through the use of accessible strain, stress, and displacement variables only. One of the advantages of the present approach is that it can treat FE software as a black-box without accessing its internal database. Furthermore, the present procedure is applicable to any type of enhanced element in tailored FE code without in-depth knowledge of the enhanced finite element formulation of interest.

Many theoretical issues should be addressed so that a stress-based topology optimization method can be successful. First, the singularity issue of the stress defined at each finite element should be resolved [3,5,10]. When the density design variables of the solid isotropic material with penalization (SIMP) topology optimization method converge to the lower bound simulating the material properties of void regions, the corresponding elements can experience excessive distortions and exhibit some non-zero stress values that cause the singularity issue of stress-based topology optimization [5]. Note that from a physical point of view, the stress values of these elements of void regions should be zero. To overcome this singularity issue, many innovative relaxation schemes such as the epsilon-relaxation method [5], the qp -relaxation method [1,7], and the relaxed stress indicator [17] approach have been proposed. Second, the local behavior of the stress constraints defined at each element should be carefully implemented from an optimization point of view [17–19]. In other words, with the stress constraints defined at all elements, it is almost impossible to solve an optimization problem with refined element-wise stress constraints within a moderate computation time. From an optimization point of view, this issue is related to the efficiency of a dual optimizer with multiple constraints as design variables. Therefore, so-called global constraint approaches have been developed to constrain only the maximum stress value to be less than a certain limiting stress value. In global constraint approaches, the aggregation function [9,20], the p -norm [1] and segregated global stress norms [9–11] have been employed. Third, the highly nonlinear behavior of the stress constraints should be addressed [6,10]. To deal with such nonlinear behavior, an accurate and efficient gradient-based optimizer should be employed. In addition to the above three issues, we found that the most relevant studies are based on in-house FE codes with two-dimensional regular plane stress elements. One of the reasons for this finding may be that the sensitivity analysis of stress constraints requires a large amount of essential internal FE information that is generally not accessible in tailored finite element codes. Another reason may be that it is too difficult to implement sensitivity analysis in more general finite element formulations. Thus, in our opinion, efforts should be made to adopt stress-based topology optimization in the framework of tailored finite element codes.

It is important to conduct stress-based topology optimization in the framework of tailored finite element codes, which normally do provide some basic information such as the structural displacement, stress, and strain. However, to compute the sensitivity values of global stress constraints, it is essential to obtain internal finite element information such as the shape function, the strain–displacement matrix, and the element stiffness matrix. What we want to emphasize is that, because of this characteristic, stress-based topology optimization in the framework of a well-established tailored finite element code has rarely been attempted. In our opinion, it would be helpful if it were possible to use a tailored finite element code without any modification or in-depth understanding of the code. To achieve this goal, we present a novel and efficient approach to retrieve some essential information required in the sensitivity analyses of general finite elements. In other words, we will challenge the notion that it is difficult to conduct stress-based topology optimization without direct access to internal finite element information.

To achieve the objective of this research, the implementation scheme of the primal analysis for structural analysis, the adjoint analysis for the Lagrangian multiplier, and the semi-sensitivity analysis in the framework of the SIMP method are employed; these approaches are represented as gray boxes in Fig. 1. Note that the finite element analysis procedure is treated as a black-box providing the basic information of various irregular finite elements. In the present implementation scheme, a key step is to calculate strain–displacement matrices for irregular FE meshes because the stress constraints require these matrices in the sensitivity analysis. Such matrices are generally not provided by commercial software, and an in-depth understanding and modification of the sophisticated open FE code is required. In the case of regular meshes, it is possible to indirectly and efficiently calculate these matrices by the finite difference method of strains with small perturbations of structural displacements. However, in the case of a finite element model with irregular-shaped meshes, obtaining the matrices is a difficult and time consuming process. Thus, we developed a new node selection procedure that allows for the efficient calculation of strain–displacement matrices for irregular FE meshes. One of the advantages of the proposed scheme is its applicability to 2D, 3D, and even shell finite elements.

This paper is organized as follows. The stress-based topology optimization formulation based on the SIMP method and analytical sensitivity analyses of the segregated global stress constraints are explained in Section 2. Some issues that arise when implementing stress-based topology optimization in the framework of tailored finite element code are also discussed. In Section 3, the novel procedure to resolve the issues outlined in the previous section is developed. Specifically, the approach

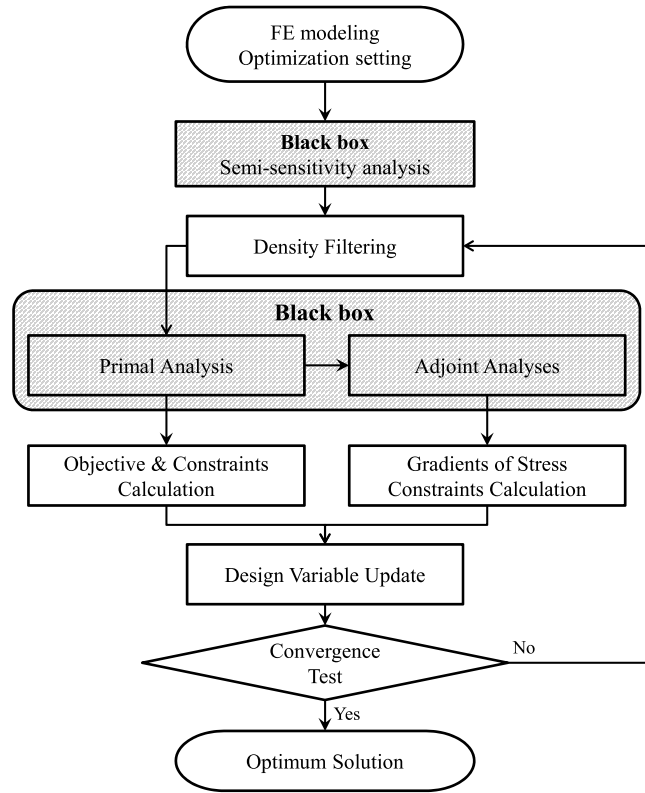


Fig. 1. Stress-based topology optimization framework with tailored finite element code.

shown in Fig. 1 for the calculation of the strain–displacement matrices for irregular finite elements is explained. In Section 4, some topology optimization problems are solved in two- and three-dimensional finite models so as to demonstrate the validity and versatility of the present approach. One set of results is compared with that obtained from Optistruct. Finally, conclusions derived from the research are presented in Section 5.

2. Stress-based topology optimization formulation and analytical sensitivity analysis

In this section, a brief explanation of the stress-based topology optimization formulation and the analytical sensitivity analysis are presented [10,21].

2.1. Stress-based topology optimization formulation

In this subsection, the topology optimization formulation considering the von Mises stress constraints defined at each finite element is described. The original topology optimization problem to minimize volume subject to von Mises stress constraints can be formulated as follows.

$$\begin{aligned}
 &\text{Minimize}_{\boldsymbol{\gamma}} \quad V(\boldsymbol{\gamma}) = \sum_{e=1}^{NE} \gamma_e v_e, \quad \boldsymbol{\gamma} = [\gamma_1, \gamma_2, \dots, \gamma_{NE}] \\
 &\text{subject to} \quad \frac{\sigma_e}{\sigma^*} \leq 1, \quad \text{if the } e\text{th element exists } (e = 1, 2, \dots, NE) \\
 &\quad \quad \quad \mathbf{KU} = \mathbf{F} \\
 &\quad \quad \quad \varepsilon \leq \gamma_e \leq 1 \quad (\varepsilon : \text{a small positive value})
 \end{aligned} \tag{1}$$

where the design variables assigned to NE elements of the design domain are denoted by $\boldsymbol{\gamma}$ when the solid isotropic material with penalization (SIMP) method is used. Note that the von Mises stress of e th element, σ_e , should be lower than the limit stress, σ^* .

For the stress-based topology optimization, the following static analysis is conducted

$$\mathbf{KU} = \mathbf{F} \tag{2}$$

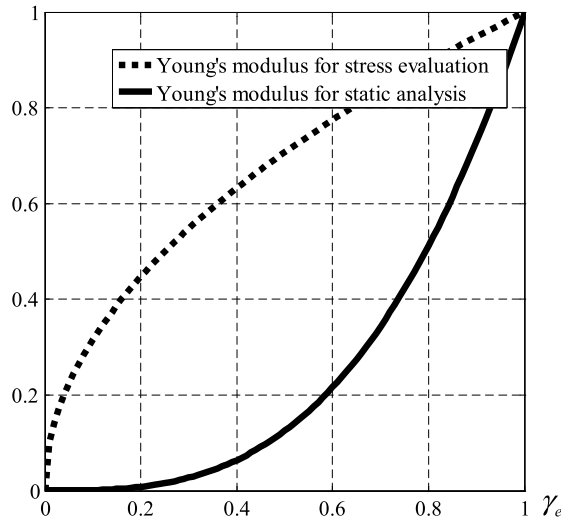


Fig. 2. Interpolations of Young's modulus for stress evaluation and for static analysis.

where the global stiffness matrix, the displacement vector, and the external forces are denoted as \mathbf{K} , \mathbf{U} , and \mathbf{F} , respectively. To generate a global stiffness matrix, the following assembly procedure is performed:

$$\mathbf{K} = \sum_{e=1}^{NE} \mathbf{A}_e \mathbf{k}_e \quad \text{and} \quad \mathbf{k}_e = \int_{v_e} \mathbf{B}^T \mathbf{C}_e \mathbf{B} dv \quad (v_e : \text{the } e\text{th element domain}) \quad (3)$$

where the symbol \mathbf{A} represents the finite element assembly operator of the e -th element stiffness matrix \mathbf{k}_e , and the strain–displacement matrix is denoted by \mathbf{B} . The constitutive matrix of the e th element \mathbf{C}_e in the SIMP method is interpolated as follows:

$$\mathbf{C}_e = \gamma_e^n \mathbf{C}_0 \quad (4)$$

where the penalization parameter and the constitutive matrix without penalization are denoted as n and \mathbf{C}_0 , respectively. Note that a value between 3 and 5 is used for n . After the structural analysis for the calculation of displacements, the element-wise stresses and von Mises stress of a finite element are evaluated as:

$$\boldsymbol{\sigma}_e = {}_s\mathbf{C}_e \mathbf{B}_e \mathbf{u}_e \quad (5)$$

$${}_s\mathbf{C}_e = \gamma_e^{n_s} \mathbf{C}_0 \quad (6)$$

$$\sigma_e = \frac{1}{\sqrt{2}} \left[(\sigma_x - \sigma_y)^2 + (\sigma_y - \sigma_z)^2 + (\sigma_z - \sigma_x)^2 + 6(\tau_{xy}^2 + \tau_{yz}^2 + \tau_{xz}^2) \right]^{1/2} \quad (7)$$

where the constitutive matrix and the penalization parameter for the stress evaluation are denoted as ${}_s\mathbf{C}_e$ and n_s , respectively. As shown in Fig. 2, the different penalization parameters are used for Young's modulus of stress evaluation, n_s , and for Young's modulus of static analysis, n . A value of 0.5 is used for n_s , which is different from the n employed in the displacement calculation to avoid the singularity problem that arises in stress-based topology optimization [10,21]. Note that the nominal von Mises stress of e th element, σ_e is calculated by using the component of element stress vector, $\boldsymbol{\sigma}_e$ in Eq. (5).

To deal with the numerous local constraints and the nonlinear characteristics of the stress constraints, the original topology optimization problem that minimizes the volume subject to the von Mises stress constraints is reformulated by introducing the regional scheme or the aggregation scheme of the element-wise constraints, as well as the p -norm approximation developed in [10,21] as follows:

$$\begin{aligned} &\underset{\gamma}{\text{Minimize}} && V(\tilde{\gamma}) = \sum_{e=1}^{NE} \tilde{\gamma}_e v_e \quad (\tilde{\gamma} : \text{Filtered density}) \\ &\text{subject to} && \langle \sigma_{\max} \rangle_1 \leq 1 \\ & && \langle \sigma_{\max} \rangle_2 \leq 1 \\ & && \vdots \\ & && \langle \sigma_{\max} \rangle_{RN} \leq 1 \\ & && \mathbf{KU} = \mathbf{F} \end{aligned} \quad (8)$$

$$\langle \sigma_{\max} \rangle_k \equiv c_k^{\text{iter}} \langle \sigma_{PN} \rangle_k \quad (e \in \Omega_k) \quad (9)$$

$$\langle \sigma_{PN} \rangle_k \equiv \left(\sum_e \left(\frac{\sigma_e}{\sigma^*} \right)^p \tilde{\gamma}_e \right)^{1/p} \quad (e \in \Omega_k) \quad (10)$$

$$c_k^{iter} = \alpha \frac{\sigma_{\max,k}^{iter-1} / \sigma^*}{\langle \sigma_{PN} \rangle_k^{iter-1}} + (1 - \alpha) c_k^{iter-1}. \quad (11)$$

Note that the density filtering scheme [22] is adopted to avoid the checkerboard issue, and the filtered design variables are denoted as $\tilde{\gamma}$. The original optimization problem is to minimize the mass usage, i.e., the sum of the multiplication of each element's volume v_e and the filtered design variable $\tilde{\gamma}_e$, subject to local stress constraints. The local stress constraints are reformulated by the regional stress constraints $\langle \sigma_{\max} \rangle_k$ with the normalized stress p -norm of the k th region $\langle \sigma_{PN} \rangle_k^{iter}$ and the correction factor c_k^{iter} . The correction parameter is calculated by considering the ratio between the normalized stress p -norm and the real maximum normalized stress value $\sigma_{\max,k}^{iter-1} / \sigma^*$ in the previous $iter-1$ optimization iteration at the k th region. The number of regions for the normalized stress p -norm calculation and the damping factor are denoted as RN and α respectively. The region for normalized stress p -norm calculation, Ω_k , is defined by considering the magnitude of von Mises stress value of each element [21].

2.2. Sensitivity analysis

To conduct stress-based topology optimization using a gradient-based optimizer, the sensitivity values of the responses, i.e., the objective and constraints, should be calculated. The sensitivities of the objective function in (8) can be easily calculated, but the calculation of the sensitivities of the stress constraints is more complicated. By using the chain rule, the sensitivities of the p -norm stress can be derived as follows:

$$\frac{d \langle \sigma_{PN} \rangle_k}{d \tilde{\gamma}_e} = \frac{\partial \langle \sigma_{PN} \rangle_k}{\partial \tilde{\gamma}_e} + \frac{\partial \langle \sigma_{PN} \rangle_k}{\partial \sigma_e} \frac{\partial \sigma_e}{\partial \tilde{\gamma}_e} + \sum_{e'=1}^{NE} \frac{\partial \langle \sigma_{PN} \rangle_k}{\partial \sigma_{e'}} \frac{\partial \sigma_{e'}}{\partial \sigma_e} \frac{\partial \sigma_e}{\partial \mathbf{U}} \frac{d \mathbf{U}}{d \tilde{\gamma}_e}. \quad (12)$$

For the sake of efficiency, the adjoint variable λ_k^T for the sensitivity analysis is introduced and can be obtained from the derivatives of the static equilibrium equation as follows:

$$\mathbf{K} \frac{d \mathbf{U}}{d \tilde{\gamma}_e} = \frac{d \mathbf{F}}{d \tilde{\gamma}_e} - \frac{d \mathbf{K}}{d \tilde{\gamma}_e} \mathbf{U}, \quad \frac{d \mathbf{F}}{d \tilde{\gamma}_e} = 0 \quad (13)$$

$$\lambda_k^T = - \sum_{e'=1}^{NE} \frac{\partial \langle \sigma_{PN} \rangle_k}{\partial \sigma_{e'}} \frac{\partial \sigma_{e'}}{\partial \sigma_e} \frac{\partial \sigma_e}{\partial \mathbf{U}} \mathbf{K}^{-1} \quad (14)$$

$$\mathbf{K}^T \lambda_k = - \sum_{e'=1}^{NE} \frac{\partial \langle \sigma_{PN} \rangle_k}{\partial \sigma_{e'}} \left(\frac{\partial \sigma_{e'}}{\partial \sigma_e} \frac{\partial \sigma_e}{\partial \mathbf{U}} \right)^T. \quad (15)$$

It is assumed that the external force is independent of the density design variables. By substituting (13)–(15) into (12), the sensitivity value of the p -norm of the von Mises stresses can be derived with the adjoint variable λ_k^T such that

$$\frac{d \langle \sigma_{PN} \rangle_k}{d \tilde{\gamma}_e} = \frac{\partial \langle \sigma_{PN} \rangle_k}{\partial \tilde{\gamma}_e} + \frac{\partial \langle \sigma_{PN} \rangle_k}{\partial \sigma_e} \frac{\partial \sigma_e}{\partial \tilde{\gamma}_e} + \lambda_k^T \frac{d \mathbf{K}}{d \tilde{\gamma}_e} \mathbf{U}. \quad (16)$$

The terms in (14) and (16) are derived as follows.

$$\frac{\partial \langle \sigma_{PN} \rangle_k}{\partial \tilde{\gamma}_e} = \frac{1}{p} \left(\sum_e \left(\frac{\sigma_e}{\sigma^*} \right)^p \tilde{\gamma}_e \right)^{\frac{1}{p}-1} \left(\frac{\sigma_e}{\sigma^*} \right)^p \quad (17)$$

$$\frac{\partial \langle \sigma_{PN} \rangle_k}{\partial \sigma_e} = \left(\sum_e \left(\frac{\sigma_e}{\sigma^*} \right)^p \tilde{\gamma}_e \right)^{\frac{1}{p}-1} \tilde{\gamma}_e \left(\frac{\sigma_e}{\sigma^*} \right)^{p-1} \frac{p}{\sigma^*} \quad (18)$$

$$\frac{\partial \sigma_e}{\partial \tilde{\gamma}_e} = \frac{n_s}{\tilde{\gamma}_e} \sigma_e \quad (19)$$

$$\frac{d \mathbf{K}}{d \tilde{\gamma}_e} \mathbf{U} = \frac{n}{\tilde{\gamma}_e} \mathbf{k}_e \mathbf{u}_e = \frac{n}{\tilde{\gamma}_e} \mathbf{f}_e \quad (20)$$

$$\frac{\partial \sigma_e}{\partial \mathbf{U}} = \frac{\partial \sigma_e}{\partial \mathbf{U}_e} = \tilde{\gamma}_e^{n_s} \mathbf{C}_0 \mathbf{B}. \quad (21)$$

Note that \mathbf{f}_e in (20) represents the internal force of the e -th element. The information needed for the calculation of (17)–(20) is directly provided from an analysis result, but most commercial FE software does not directly provide the matrix $\mathbf{C}_0\mathbf{B}$ in (21). Therefore, to obtain these matrices indirectly using only analysis results from the FE software, a semi-analytic approach is developed in the next section.

3. Implementation of stress-based topology optimization in a tailored finite element software package

As stated in Section 2.2, one of the major difficulties in implementing sensitivity analysis in the framework of tailored FE codes is that internal FE data, such as the $\mathbf{C}_0\mathbf{B}$ matrices, may only be accessed by engineers and scientists with some in-depth modifications of the FE code itself. To overcome this major difficulty, a new computational procedure that is inexpensive from a computational point of view is now presented. For the sake of simplicity, we first develop the procedure for a plane stress element (2-dimensional in-plane element) and then expand it to general finite element formulations (plate, shell, and three-dimensional elements).

3.1. Fast calculations of $\mathbf{C}_0\mathbf{B}$ matrices using the displacement perturbation approach

We found that all terms except $\mathbf{C}_0\mathbf{B}$ in (12) can be easily calculated with commonly provided FE post-processing information such as the stress components, strain components, and displacement values. First, the partial differentiation of the p -norm stress with respect to the filtered design variables can be explicitly derived by the mathematical definitions of (17). The components of the second right term of (12) also can be computed analytically by the definitions of the p -norm stress, the von Mises stress, and the stress interpolation scheme. However, the derivation of the third term on the right side of (12) becomes complicated due to the components of $\mathbf{C}_0\mathbf{B}$, which are related to the type of FE elements of interest and are difficult to access in tailored FE software packages. In other words, computations of the third term of (12) require an in-depth understanding of the finite element itself and thus, an employed finite element code is usually reprogrammed to provide the terms directly. What we should emphasize is that, in order to incorporate tailored FE software, it is important to calculate this sensitivity value in (12). To the best of our best knowledge, indirect or semi-analytical calculations outside of tailored FE software without any modification to the code have been regarded as impossible because of the heavy computational load. Thus, this section is devoted to overcoming this biased opinion.

In order to calculate $\mathbf{C}_0\mathbf{B}$ semi-analytically with only stress and strain values, it is first noted that this term is the partial derivative of an element stress vector with respect to structural displacements as follows

$$\frac{\partial \boldsymbol{\sigma}_e}{\partial \mathbf{U}} = \frac{\Delta \boldsymbol{\sigma}_e}{\Delta \mathbf{U}} = \begin{bmatrix} \frac{\Delta \sigma_{x,1}}{\Delta U_{x,1}} & \frac{\Delta \sigma_{y,1}}{\Delta U_{y,1}} & \frac{\Delta \sigma_{z,1}}{\Delta U_{z,1}} & \frac{\Delta \sigma_{rx,1}}{\Delta U_{rx,1}} & \frac{\Delta \sigma_{ry,1}}{\Delta U_{ry,1}} & \frac{\Delta \sigma_{rz,1}}{\Delta U_{rz,1}} & \dots \\ \frac{\Delta \sigma_{x,eND}}{\Delta U_{x,eND}} & \frac{\Delta \sigma_{y,eND}}{\Delta U_{y,eND}} & \frac{\Delta \sigma_{z,eND}}{\Delta U_{z,eND}} & \frac{\Delta \sigma_{rx,eND}}{\Delta U_{rx,eND}} & \frac{\Delta \sigma_{ry,eND}}{\Delta U_{ry,eND}} & \frac{\Delta \sigma_{rz,eND}}{\Delta U_{rz,eND}} \end{bmatrix} \quad (22)$$

where the stress perturbations of the e th element with the perturbed displacement vector $\Delta \mathbf{U}_{(O),i}$ (the perturbing i -th component of the displacement vector of the e th element) are $\Delta \boldsymbol{\sigma}_{(O),i}$. The subscripts rx , ry , and rz denote x , y , and z rotations, respectively. The number of nodes of the e th element is eND .

Without loss of generality, let us consider a four-node plane stress element. By assuming a linear material and small displacements, the above term (a 3 by 8 matrix) is simplified as follows:

$$\frac{\partial \boldsymbol{\sigma}_e}{\partial \mathbf{U}} = \begin{bmatrix} \frac{\Delta \sigma_{x,1}}{\Delta U_{x,1}} & \frac{\Delta \sigma_{y,1}}{\Delta U_{y,1}} & \frac{\Delta \sigma_{x,2}}{\Delta U_{x,2}} & \frac{\Delta \sigma_{y,2}}{\Delta U_{y,2}} & \frac{\Delta \sigma_{x,3}}{\Delta U_{x,3}} & \frac{\Delta \sigma_{y,3}}{\Delta U_{y,3}} & \frac{\Delta \sigma_{x,4}}{\Delta U_{x,4}} & \frac{\Delta \sigma_{y,4}}{\Delta U_{y,4}} \end{bmatrix} \quad (23)$$

where $\Delta U_{(O),i}$ and $\Delta \boldsymbol{\sigma}_{(O),i}$ are the perturbation of the i -th node displacement in the (O) direction ($O = x$ or y) and the corresponding perturbation of the e th element stress vector (represented by a column vector), respectively. To develop an efficient numerical procedure for this term, we note the following:

Remark 1. The above relationships between the stress and displacements, (22) and (23), are satisfied for any finite element formulation with a linear analysis.

Remark 2. The above matrix values of (23) become constants in the case of a linear analysis if the design variable values are fixed. Thus, it is possible to calculate the above matrix values by perturbing displacement values without a global stiffness matrix inversion, as shown in Fig. 3. Furthermore, the process of assigning and perturbing artificial displacements does provide the same strain–displacement matrices (no FE matrix inversion).

Remark 3. Stress calculations with perturbed structural displacements require heavier computations. For example, let us consider a finite element model consisting of irregular-shaped linear plane stress elements with nd nodes. To compute the $\mathbf{C}_0\mathbf{B}$ matrices for all finite elements with $nd \times 2$ degrees of freedom, $nd \times 2$ post-processing procedures are required, which inevitably leads to a finite element procedure with a tremendous computational load.

In order to reduce the computational cost of the above sensitivity analysis for the $\mathbf{C}_0\mathbf{B}$ matrix, we present a novel semi-sensitivity analysis approach. In this analysis procedure, it is noted that there are some node sets whose displacement

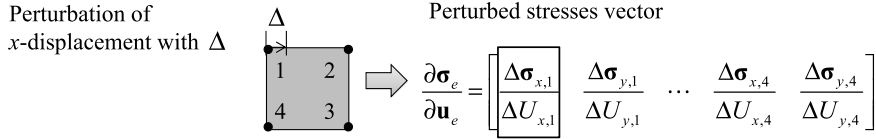


Fig. 3. The semi-sensitivity analysis for the $\mathbf{C}_0\mathbf{B}$ matrix.

perturbations influence only one column of each element's partial derivative matrix. By perturbing the displacements of all nodes of one node set simultaneously and calculating the strain–displacement matrices for the elements associated with one node set simultaneously, it is possible to reduce computation times. To make this point clear, let us consider a simple finite model with 9 regular 4-node elements, as shown in Fig. 4. To compute the strain–displacement matrices efficiently, the semi-analytical method in Fig. 3 is employed. First, the perturbations of the displacements of the first, third, tenth, and twelfth nodes (hereafter referred to as the first node set) affect only one column of each element's partial derivative matrix. Using this relationship, the x and y displacements of the nodes of the first node set are simultaneously perturbed to compute one column of $\mathbf{C}_0\mathbf{B}$ matrix of each element associated with the first node set. For the other columns of $\mathbf{C}_0\mathbf{B}$ matrices, we define the second and third node sets and perturb the displacements as in the case of the first node set.

It is important to notice that the above procedures do not require stiffness matrix inversions; only the post-processing procedure providing element stress values is needed (see Remark 2). For example, without the present node set algorithm, 32 post-processing steps are required because the number of degrees of freedom of the FE model of interest is 32. However, with the present node set algorithm, only 8 FE post-processing steps (no FE inversion, see Remark 2) are required.

3.2. Node set generation algorithm

To automatically generate the node sets, the connectivity information in Fig. 4 is used. In this research, we developed the following automatic node set generation algorithm. The detailed procedures of the above steps for the finite element model of Fig. 4 are presented in Table 1.

NODE SET GENERATION ALGORITHM (NS: Node set, CNS: Current node set, ENS: Exclude node set)

Step 1: Search all connectivity information of the given finite elements in order to select the first appearing node that does not belong to both the current node set (CNS) and the node set (NS). The node set (NS) is a set of nodes whose displacement perturbations do not influence the stress values of other elements whose nodes do not belong to the current node set. The current node set (CNS) is an auxiliary node set and will be added to the node set (NS) after Steps 2, 3, and 4. At the first step, the current node set is initialized to null.

Step 2: If the nodes consisting of a current element do not belong to the current node set (CNS), save the indices of the nodes consisting of the current element into the exclude node set (ENS). After determining all elements whose nodes are members of the current node set (CNS), all nodes of the current element that are not members of the current node set (CNS) are inserted into the exclude node set (ENS).

Step 3: For all elements, add all nodes satisfying the following sub-steps into CNS or ENS.

Sub-step 3-1: Select all nodes of a current element that are not included in the node set (NS) or the exclude node set (ENS) and save them to the temporary node set (TEMP_NS). If all nodes of the current element are members of the node set (NS) or the current node set (CNS), consider the next element.

Sub-step 3-2: If any member of the temporary node set (TEMP_NS) is a member of the current node set, ignore the temporary node set (TEMP_NS). If not, the first member of the temporary node set is added to the current node set and the other members of the temporary node set are added to the exclude node set (ENS).

Sub-step 3-3: Search all elements containing the newly added node at criterion 3. Then, determine all nodes among the searched elements that do not belong to the current node set and save them to the eliminate node set (ENS).

Sub-step 3-4: Add the current node set (CNS) into the node set (NS). If all nodes are selected, then exit. If not, initialize the eliminate node set (ENS) and the current node set (CNS) and go to Step 1.

To demonstrate the applications of the present node set selection algorithm in Table 1, the scheme is applied to several illustrative 2D and 3D models in Fig. 5. Note that these models are intentionally meshed irregularly or regularly.

Shown in Table 2 are the node set number and node sets generated with the present node set selection algorithm. Although it cannot be generalized or proven mathematically, the numbers of the node sets for regular FE meshes tend to be same as the number of nodes per element. For the case of irregular FE meshes, it is likely that the number of node sets becomes larger than the number of nodes per element. In addition, the number of node sets is dependent on the node number scheme.

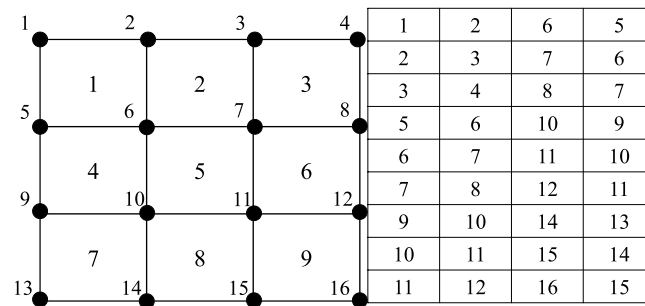


Fig. 4. A simple FE model and its element table (the first node set: 1, 3, 10, 12, the second node set: 2, 4, 9, 11, the third node set: 6, 8, 14, 16, the fourth node set: 5, 7, 13, 15).

Table 1

Node set selection example for the FE model in Fig. 4 (iELM: element index, {}: null).

iELM	NS	TNS	CNS	ENS
1	{}		1	2, 6, 5
2	{}	3, 7	1, 3	2, 6, 5, 7, 4, 8
3	{}	3	1, 3	2, 6, 5, 7, 4, 8
4	{}	10, 9	1, 3, 10	2, 6, 5, 7, 4, 8, 9, 11
5	{}	10	1, 3, 10	2, 6, 5, 7, 4, 8, 9, 11
6	{}	12	1, 3, 10, 12	2, 6, 5, 7, 4, 8, 9, 11, 15, 16
7	{}	10, 14, 13	1, 3, 10, 12	2, 6, 5, 7, 4, 8, 9, 11, 15, 16, 14, 13
8	{}	10	1, 3, 10, 12	2, 6, 5, 7, 4, 8, 9, 11, 15, 16, 14, 13
9	{}	12	1, 3, 10, 12	2, 6, 5, 7, 4, 8, 9, 11, 15, 16, 14, 13
1	{1, 3, 10, 12}			
2	{1, 3, 10, 12}		2	1, 6, 5, 3, 7
3	{1, 3, 10, 12}	2	2	1, 6, 5, 3, 7
4	{1, 3, 10, 12}	4, 8	2, 4	1, 6, 5, 3, 7, 8
5	{1, 3, 10, 12}	9	2, 4, 9	1, 6, 5, 3, 7, 8, 10, 14, 13
6	{1, 3, 10, 12}	11	2, 4, 9, 11	1, 6, 5, 3, 7, 8, 10, 14, 13, 12, 15, 16
7	{1, 3, 10, 12}	11	2, 4, 9, 11	1, 6, 5, 3, 7, 8, 10, 14, 13, 12, 15, 16
8	{1, 3, 10, 12}	9	2, 4, 9, 11	1, 6, 5, 3, 7, 8, 10, 14, 13, 12, 15, 16
9	{1, 3, 10, 12}	11	2, 4, 9, 11	1, 6, 5, 3, 7, 8, 10, 14, 13, 12, 15, 16
1	{1, 3, 10, 12}, {2, 4, 9, 11}			
2	{1, 3, 10, 12}, {2, 4, 9, 11}		6	1, 2, 5, 3, 7, 10, 9, 11
3	{1, 3, 10, 12}, {2, 4, 9, 11}	6	6	1, 2, 5, 3, 7, 10, 9, 11, 4, 12
4	{1, 3, 10, 12}, {2, 4, 9, 11}	8	6, 8	1, 2, 5, 3, 7, 10, 9, 11, 4, 12
5	{1, 3, 10, 12}, {2, 4, 9, 11}	6	6, 8	1, 2, 5, 3, 7, 10, 9, 11, 4, 12
6	{1, 3, 10, 12}, {2, 4, 9, 11}	8	6, 8	1, 2, 5, 3, 7, 10, 9, 11, 4, 12
7	{1, 3, 10, 12}, {2, 4, 9, 11}	14, 13	6, 8, 14	1, 2, 5, 3, 7, 10, 9, 11, 4, 12, 13, 15
8	{1, 3, 10, 12}, {2, 4, 9, 11}	14	6, 8, 14	1, 2, 5, 3, 7, 10, 9, 11, 4, 12, 13, 15
9	{1, 3, 10, 12}, {2, 4, 9, 11}	16	6, 8, 14, 16	1, 2, 5, 3, 7, 10, 9, 11, 4, 12, 13, 15
1	{1, 3, 10, 12}, {2, 4, 9, 11}, {6, 8, 14, 16}			
2	{1, 3, 10, 12}, {2, 4, 9, 11}, {6, 8, 14, 16}		5	1, 2, 6, 10, 9
3	{1, 3, 10, 12}, {2, 4, 9, 11}, {6, 8, 14, 16}	7	5, 7	1, 2, 6, 10, 9, 3, 4, 8, 11, 12
4	{1, 3, 10, 12}, {2, 4, 9, 11}, {6, 8, 14, 16}	7	5, 7	1, 2, 6, 10, 9, 3, 4, 8, 11, 12
5	{1, 3, 10, 12}, {2, 4, 9, 11}, {6, 8, 14, 16}	5	5, 7	1, 2, 6, 10, 9, 3, 4, 8, 11, 12
6	{1, 3, 10, 12}, {2, 4, 9, 11}, {6, 8, 14, 16}	7	5, 7	1, 2, 6, 10, 9, 3, 4, 8, 11, 12
7	{1, 3, 10, 12}, {2, 4, 9, 11}, {6, 8, 14, 16}	7	5, 7	1, 2, 6, 10, 9, 3, 4, 8, 11, 12
8	{1, 3, 10, 12}, {2, 4, 9, 11}, {6, 8, 14, 16}	13	5, 7, 13	1, 2, 6, 10, 9, 3, 4, 8, 11, 12, 14
9	{1, 3, 10, 12}, {2, 4, 9, 11}, {6, 8, 14, 16}	15	5, 7, 13, 15	1, 2, 6, 10, 9, 3, 4, 8, 11, 12, 14, 16
1	{1, 3, 10, 12}, {2, 4, 9, 11}, {6, 8, 14, 16}, {5, 7, 13, 15}	15	5, 7, 13, 15	1, 2, 6, 10, 9, 3, 4, 8, 11, 12, 14, 16

Table 2

Generated node sets for the example in Fig. 5.

Example	Number of node set	Node set
Fig. 5(a)	4	{1, 4, 5, 9, 14, 15, 27}, {2, 3, 7, 8, 13, 17, 21, 24}, {6, 11, 16, 23, 26}, and {10, 12, 18, 19, 20, 22, 25}
Fig. 5(b)	5	{4, 8, 9, 20, 24, 27}, {2, 3, 12, 17, 22, 28}, {5, 14, 16, 19, 23, 25}, {1, 7, 10, 13, 15, 21, 26}, and {6, 11, 18}
Fig. 5(c)	8	{1, 7, 12, 30, 37, 38, 40, 43}, {4, 8, 10, 26, 29, 39, 42}, {6, 11, 28, 41, 44}, {2, 3, 5, 9, 25, 27, 45}, {14, 19, 24, 36, 46, 47, 49, 52}, {15, 20, 22, 32, 35, 48, 51}, {18, 23, 34, 50, 53}, and {13, 16, 17, 21, 31, 33, 54}
Fig. 5(d)	12	{20, 23, 30, 34, 37, 42}, {17, 19, 22, 24, 35, 36}, {21, 26, 32, 40, 43, 44}, {25, 27, 28, 29, 38, 41}, {3, 10, 13, 18, 47, 53}, {9, 11, 14, 16, 54, 55}, {1, 7, 12, 46, 49, 51}, {4, 6, 8, 48, 50, 56}, {5, 31}, {15, 33, 39}, {2, 52}, and {45}

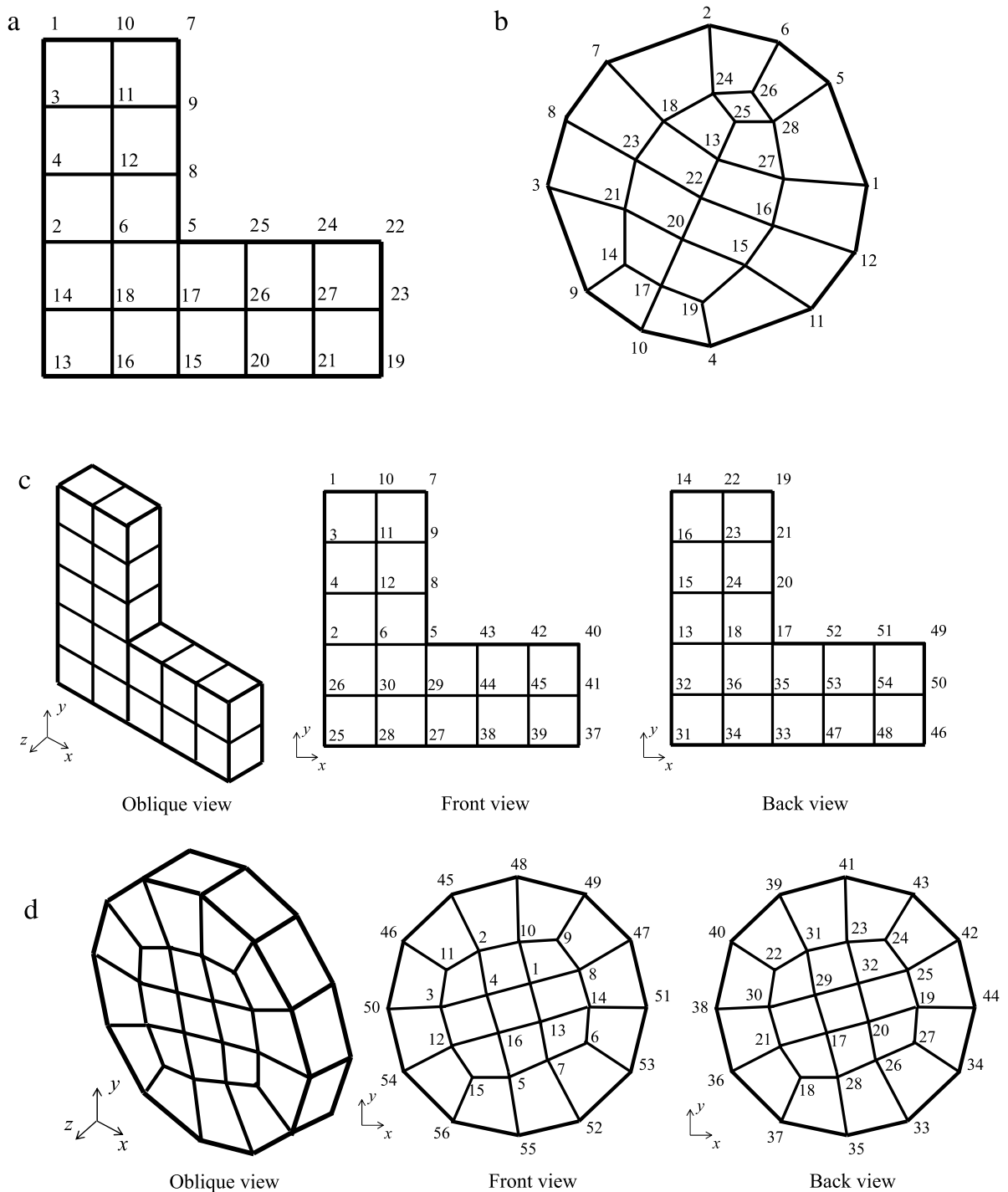


Fig. 5. Node set selection examples with various FE models. (a) 2-dimensional regular mesh, (b) 2-dimensional irregular mesh, (c) 3-dimensional regular mesh, and (d) 3-dimensional irregular mesh.

3.3. Sensitivity analysis verification

To demonstrate the accuracy and versatility of the developed sensitivity calculation procedure for tailored finite element code, we consider the cylindrical-shaped FE model in Fig. 6. The model is made with Shell 63 elements implemented in ANSYS. The cylindrical-shaped structure is fixed at the left edge and a load of 10 N is applied in the y-direction to the right edge of all nodes. To the best of our knowledge, it is impossible to directly access the detailed ANSYS information necessary

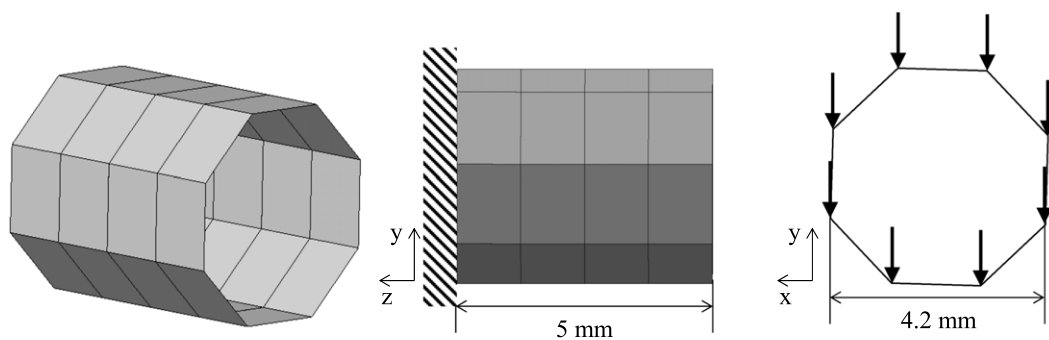


Fig. 6. A shell FE model for sensitivity verification (thickness of the shell element: 0.1 mm, Young's modulus: 210 GPa, Poisson's ratio: 0.3, $p = 4$).

Table 3

A comparison of the sensitivity values obtained with the present method and the finite difference method.

Design variable no.	Sensitivities from FDM	Sensitivities from the present method	Relative absolute error (%)	Design variable no.	Sensitivities from FDM	Sensitivities from the present method	Relative absolute error (%)
1	-0.28797	-0.28797	2.2674×10^{-5}	17	-0.28797	-0.28797	4.0619×10^{-5}
2	-0.30739	-0.30739	2.8521×10^{-5}	18	-0.30739	-0.30739	1.6037×10^{-5}
3	-0.18959	-0.18959	3.3611×10^{-5}	19	-0.18959	-0.18959	2.1039×10^{-5}
4	-0.15278	-0.15278	2.6719×10^{-5}	20	-0.15278	-0.15278	1.5401×10^{-5}
5	-0.07939	-0.07939	8.6701×10^{-5}	21	-0.07939	-0.07939	9.6391×10^{-5}
6	-0.01641	-0.01641	2.0440×10^{-4}	22	-0.01641	-0.01641	1.3807×10^{-5}
7	-0.11540	-0.11540	7.4750×10^{-5}	23	-0.11540	-0.11540	8.0277×10^{-5}
8	-0.03562	-0.03562	5.3348×10^{-5}	24	-0.03562	-0.03562	7.9915×10^{-5}
9	-0.29191	-0.29191	3.7445×10^{-5}	25	-0.29191	-0.29191	3.7057×10^{-5}
10	-0.24137	-0.24137	5.3688×10^{-5}	26	-0.24137	-0.24137	6.2873×10^{-5}
11	-0.18514	-0.18514	3.5465×10^{-5}	27	-0.18514	-0.18514	4.2582×10^{-5}
12	-0.22750	-0.22750	6.0317×10^{-5}	28	-0.22750	-0.22750	6.9595×10^{-5}
13	-0.06727	-0.06727	1.0520×10^{-4}	29	-0.06727	-0.06727	1.2771×10^{-4}
14	-0.21969	-0.21969	8.5907×10^{-5}	30	-0.21969	-0.21969	6.2944×10^{-5}
15	-0.10243	-0.10243	9.6958×10^{-5}	31	-0.10243	-0.10243	5.3588×10^{-5}
16	-0.25316	-0.25316	7.3096×10^{-5}	32	-0.25316	-0.25316	8.2085×10^{-5}

for a sensitivity analysis of the stress constraints in the framework of SIMP-based topology optimization. However, with the help of the present procedure, all necessary information, including the strain–displacement matrices, can be computed semi-analytically.

For the calculation of p -norm stress, the p value is set to 4 and the accuracy of the present method is compared with the finite difference method (FDM) with a perturbation size of 10^{-7} in Table 3. The design variables are the assigned densities of the SIMP method. A comparison of the sensitivity values computed by the present method and the finite difference method is presented in Table 3. As is evident in the table, it is possible to achieve an accurate sensitivity analysis.

3.4. The STOM framework using a commercial CAE software package

Through the use of the developed sensitivity analysis procedure, the sensitivities of the objective and constraint values can be obtained without in-depth knowledge of internal FE data. Therefore, the framework for the stress-based topology optimization procedure using commercial CAE software can be established as shown in Fig. 7. The framework can be divided into a preprocessing part and a topology optimization part. Because the information of the density filter does not change during the topology optimization, this information is calculated before optimization. For the same reason, the $\mathbf{C}_0\mathbf{B}$ matrices are calculated before optimization. The analysis results, including the displacements, stress, and internal force, are saved for calculations of the objective, the constraints, and the adjoint load. Note that all calculations for the primal analysis and the adjoint analysis are conducted in the framework of tailored finite element code.

4. Topology optimization examples

In this section, the validity of the present procedure for stress-based topology optimization is demonstrated by solving three illustrative problems: an L-shaped bracket, the control arm of a suspension system [23], and a wing rib design [23]. For tailored CAE software, the ANSYS solver is employed, but other CAE software can be used without a loss of generality. For an optimizer, the method of moving asymptotes is used [24].

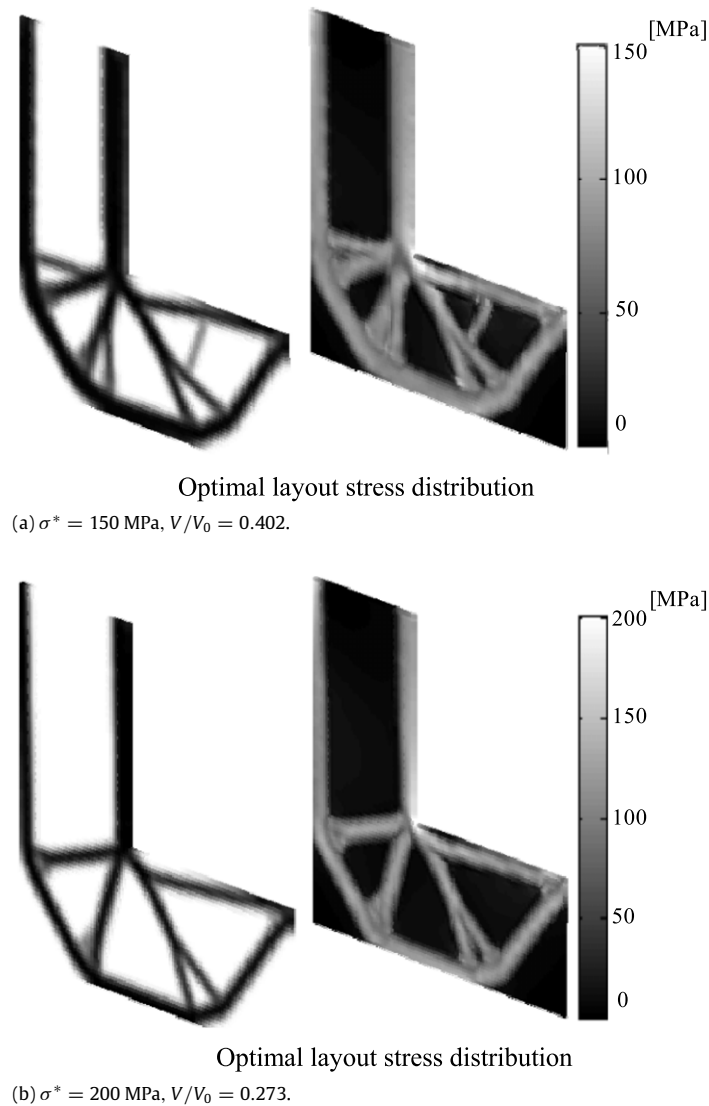


Fig. 9. The L-shaped beam results with a 1 mm thickness using $RN = 4$ and $r_{\min} = 2.5$ mm: (a) $V/V_0 = 0.273$, maximum stress = 150 MPa and (b) $V/V_0 = 0.273$, maximum stress = 200 MPa.

As the developed procedures are based on tailored FE software, it is easy to extend them to three-dimensional problems. In contrast to the compliance minimization problem [9,10,25], it is known that the reentrant corner should be smoothed in order to prevent a local stress concentration. The two domains are discretized by hexahedral isoparametric elements (1 mm \times 1 mm \times 1 mm for the left design domain and 1.25 mm \times 1.25 mm \times 1.25 mm for the right design domain due to their different thicknesses) and loads with different magnitudes (200 N and 500 N, respectively) are applied. The number of node sets for both the first domain and the second domain is eight and the number of post-processing steps needed to calculate $\mathbf{C}_0\mathbf{B}$ is 24 (number of degrees of freedom \times number of node sets = 3×8). The optimization results obtained with the present approach with different stress limitations are shown in Fig. 9. It is observed that the topological layouts are similar to those of the two-dimensional bracket designs with a small thickness of 1 mm. In addition, as the stress limit becomes larger, the mass usage becomes smaller. As observed from the two-dimensional results in Refs. [9,10,25], the reentrant corners are smoothed in order to avoid stress concentrations, which shows the validity of the present approach. The optimization results obtained with a 20 mm thickness are displayed in Fig. 10. Compared with the designs used to acquire the two-dimensional results, it is observed that the re-entrance corner is not smoothed. Instead, a triangular-shaped supporting structure appears near the corner to distribute the applied force satisfying all of the stress constraints. Note that all results are obtained without direct access to the internal FE database.

Example 2 (Control Arm of a McPherson Suspension System). To demonstrate the applicability of the present approach to irregular FE meshes and multiple loads, the control arm attached to the chassis in a McPherson suspension system

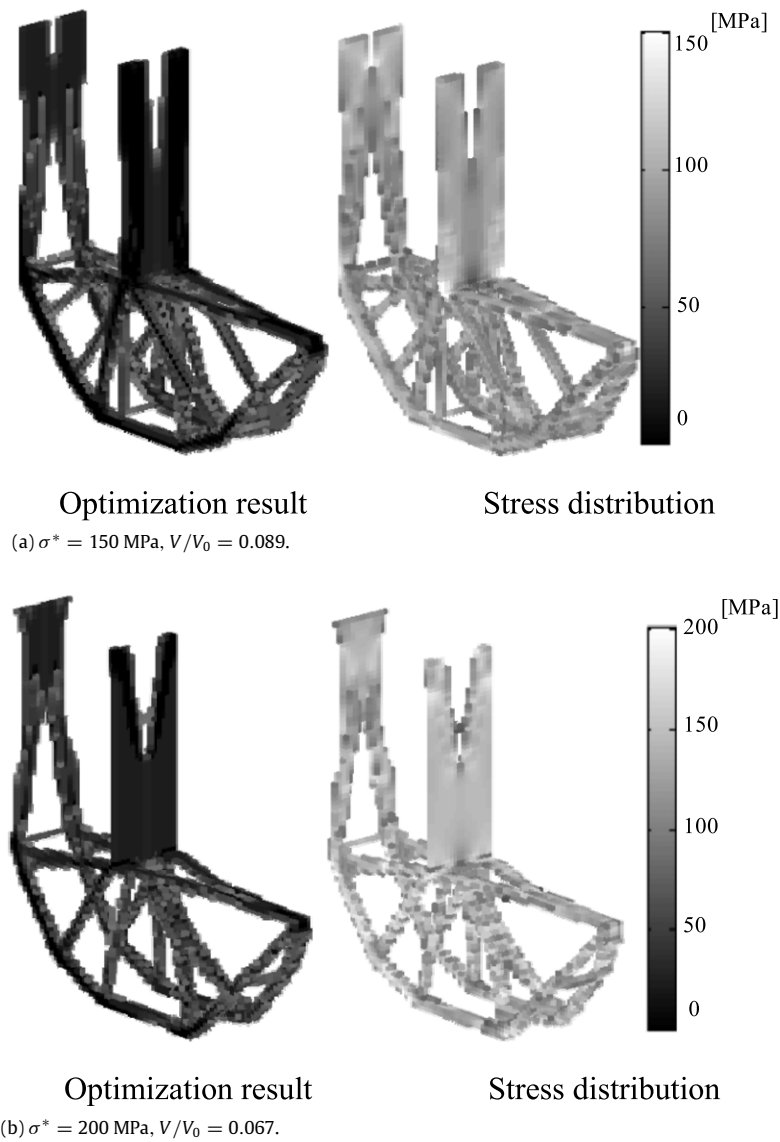


Fig. 10. The L-shaped beam results with a 20 mm thickness using $RN = 4$ and $r_{\min} = 1.5 \text{ mm}$: (a) $V/V_0 = 0.089$, maximum stress = 150 MPa, and (b) $V/V_0 = 0.067$, maximum stress = 200 MPa.

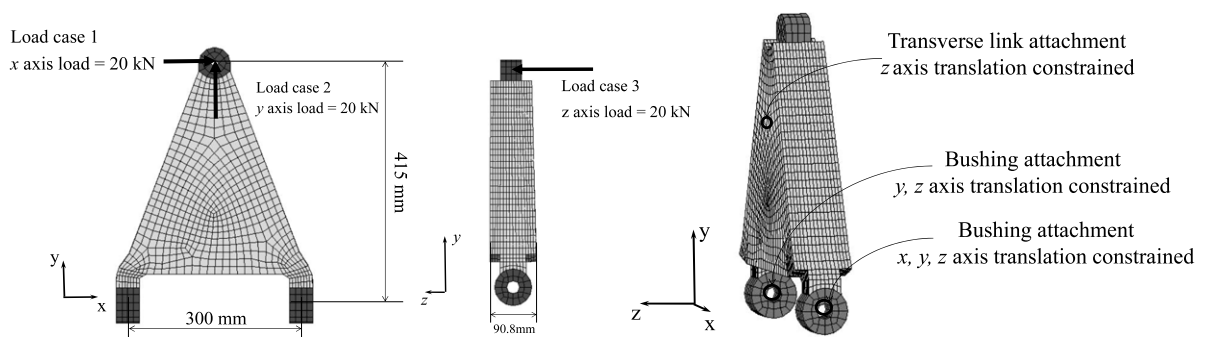


Fig. 11. The geometries, load, and support conditions of the control arm [23].

is optimized by considering the stress constraints in Fig. 11. Furthermore, to compare the optimized layouts from the present approach and Altair Optistruct, the geometry and loads of the control arm are taken from the Altair Optistruct user

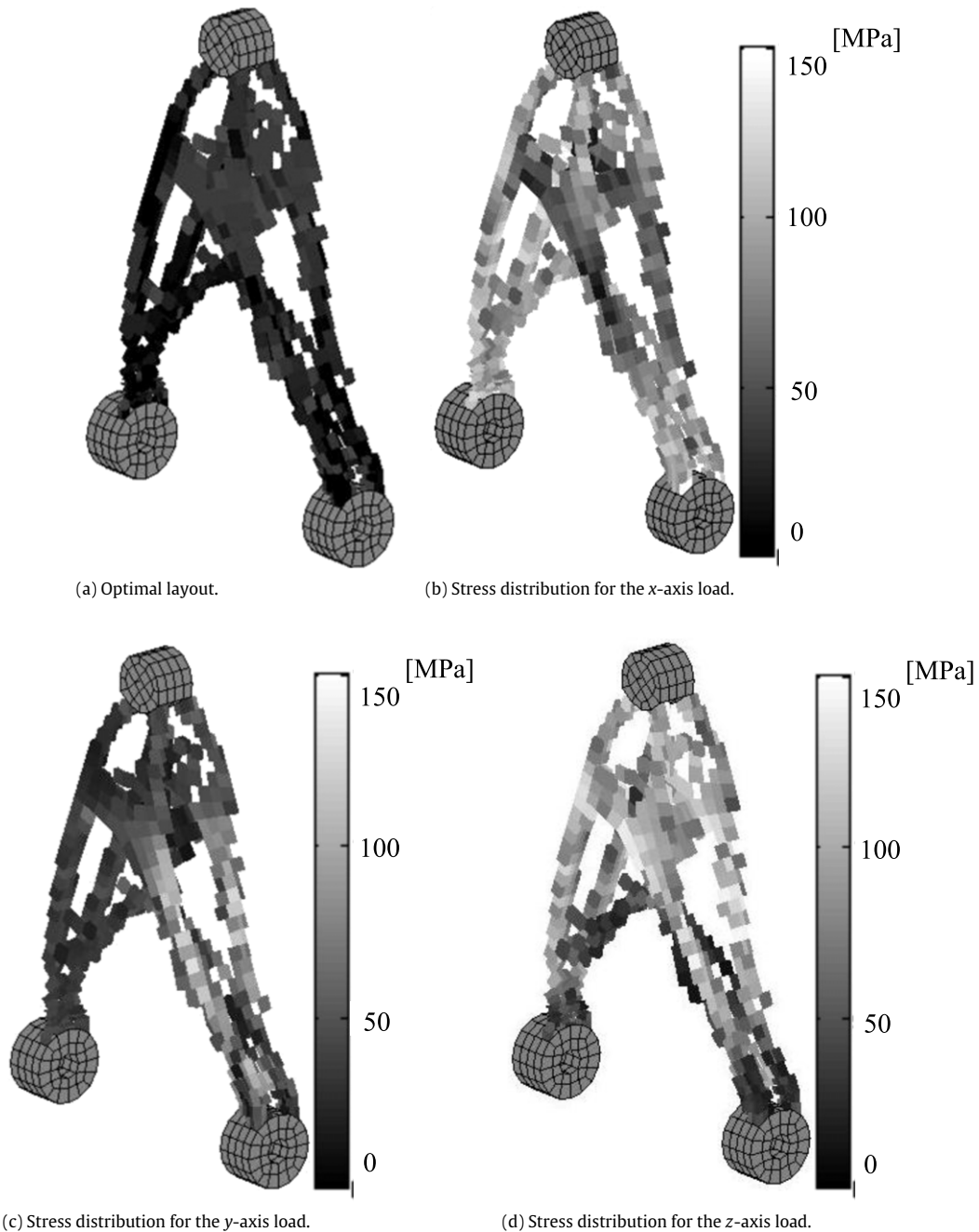


Fig. 12. The control arm of the suspension system (threshold density = 0.5, $r_{\min} = 6$ mm, $RN = 4$, $V/V_0 = 0.099$, the maximum stress for the x-axis load = 150 MPa, the maximum stress for y-axis load = 150 MPa, the maximum stress for z-axis load = 150 MPa).

manual [23]. The structure is discretized with 8304 irregular finite elements. The breaking load (x-direction), cornering load (y-direction), and driving load into a pothole (z-direction) are independently applied at the outer fastening point (multiple loading). For a rigorous optimization process, we set the number of regions as $RN = 4$, which raises the issue of how to define the regional constraints for multiple loads. To the best of our knowledge, there is no published research addressing the stress constraints for multiple loads. In this work, we simply define the regional stress constraints for each load and the number of the stress constraints becomes 12. The number of node sets for the given FE mesh is 13 and the number of post-processing calls for C_0B is 39. Shown in Fig. 12 is the optimal layout post-processed with a threshold density value of 0.5 for the sake of representation and the corresponding stress distributions for each load case. It is confirmed that all stress constraints are satisfied for all loads. To show the validity of the design, a comparison is made between the design by Optistruct with the stress constraints in Fig. 13 (the isosurface representation of the optimal layout from Optistruct post-processed with

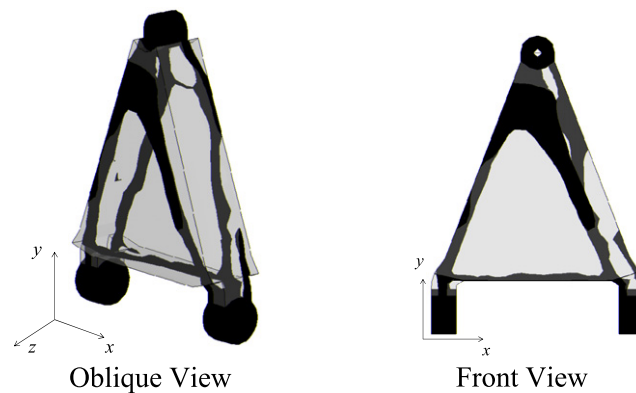


Fig. 13. Isosurface representations of the optimal layout of the control arm from Optistruct (threshold density = 0.5, $V/V_0 = 0.088$, the maximum stress for x axis load = 563.1 MPa, the maximum stress for y axis load = 80.2 MPa, the maximum stress for z axis load = 26.5 MPa).

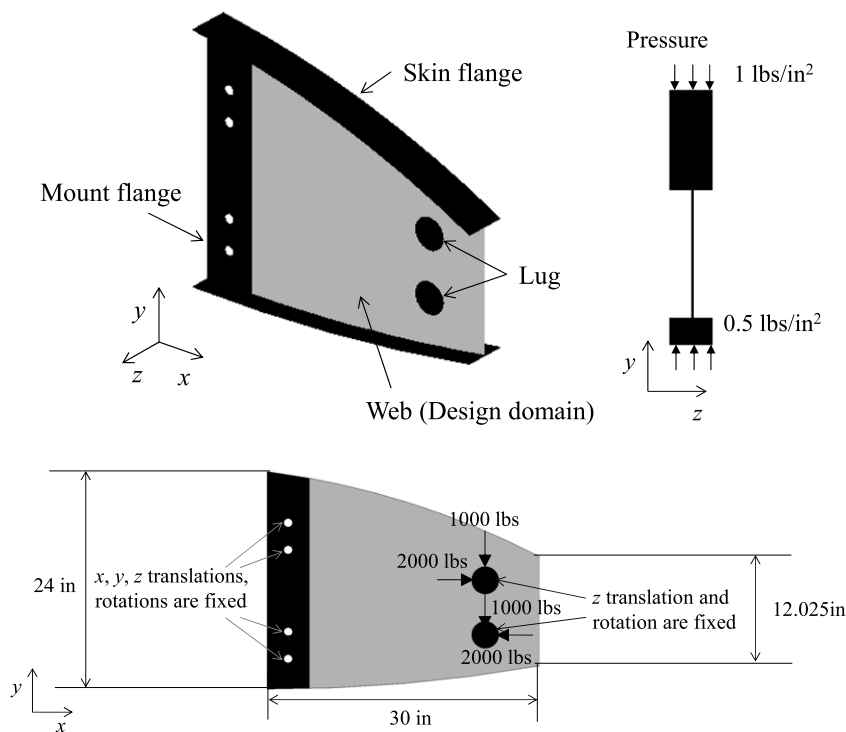


Fig. 14. The geometries, load, and support conditions of the wing rib.

a threshold density of 0.5) and the present design; similar results with some differences were obtained. The observed discrepancies are due to differences in the implemented formulation by Optistruct and the present optimization formulation. This example shows that the present procedure without direct access to the internal FE database can be applied for irregular meshes and multiple loads.

Example 3 (Wing Rib Design Example). Because the present procedure does retrieve the necessary information through a post-processing module (which is normally provided by tailored software), it is possible to apply the scheme to advanced finite elements (e.g., shell and plate elements) without knowing specific details about the finite element formulation. This feature is very handy for incorporation into tailored finite element code. To demonstrate this unique feature of the present procedure, we consider a three-dimensional wing rib model [23] with Shell 63 elements implemented in ANSYS, which is one of the problems from Altair Optistruct. Since the present procedure is allowed to retrieve some stress and strain values by ANSYS, it can be applied without difficulty.

The wing rib in Fig. 14 consists of four parts: the skin flange, the mound flange, the lug, and the web. In this numerical example, the domain of the web is set to a design domain and we distribute material in order to satisfy the stress constraints.

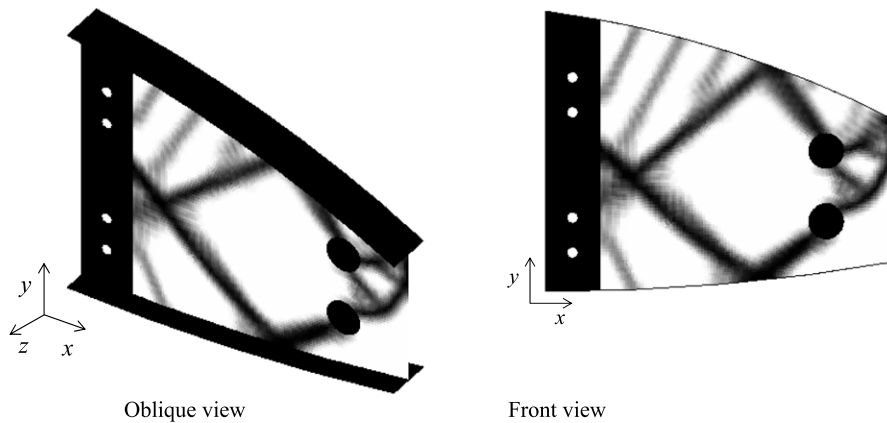


Fig. 15. An optimization result for the wing rib ($r_{\min} = 0.6$ in, $RN = 5$, $\sigma^* = 25$ kpsi, $V/V_0 = 0.240$, $\sigma_{\max} = 25$ kpsi; the stress constraints are feasible).

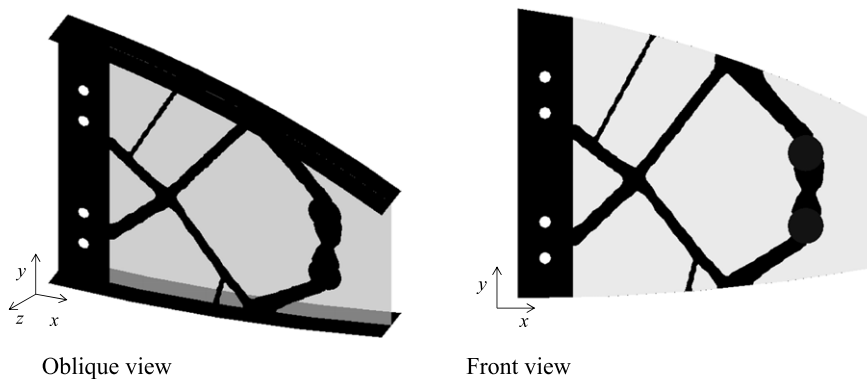


Fig. 16. Isosurface representation of an optimal layout of the wing rib from Optistruct (threshold density = 0.3, $r_{\min} = 0.6$ in, $\sigma^* = 25$ kpsi, $\sigma_{\max} = 33.1$ kpsi, $V/V_0 = 0.144$; the stress constraints are not feasible).

The displacements and rotation of the mount flange's hole are fixed, as are the z-directional translation and rotation of the nodes of the two lugs. A uniform 1 lb/in^2 pressure is applied at the upper part of the skin flange, while a uniform 0.5 lb/in^2 pressure is applied at the lower part of the skin flange. Furthermore, distributed y-directional forces are applied to the nodes at the upper and lower parts of the lug and the net forces applied to each part are 1000 lbs. Similar to the y-directional forces, distributed x-directional forces are applied to each lug and the net force is 2000 lbs. The x-directional forces applied to each part are in opposite directions, as shown in Fig. 14. Some modifications are made to the finite element model provided by Optistruct, namely, the nonlinear gap elements are erased. The number of node sets is eight and the number of post-processing calls is 48 (8×6). The topology optimization results obtained with the present optimization procedure and Altair Optistruct are shown in Figs. 15 and 16, respectively. It seems that the overall geometries obtained with the two methods are similar, but with some differences. Due to the x- and y-directional loads applied to the lugs, the two legs at the left side of the lugs appeared in Figs. 15 and 16. Obviously, some differences near the right side of the upper lug are observed due to differences in the stress-based optimization formulation. From this numerical example, it is shown that the present procedure can be applied to a finite element model with advanced finite elements without knowing detailed information such as the interpolation function and the stress–displacement matrix.

5. Conclusions

It has long been believed that it is difficult or impossible to conduct topology optimization considering the local stress constraints in the framework of tailored finite element code by only providing basic post-processing information. To challenge this belief, we developed a novel procedure that utilizes only basic finite element post-processing data for stress-based topology optimization minimizing the volume subject to local stress constraints. One of the advantages of the present procedure is that it indirectly calculates necessary information, such as the $\mathbf{C}_0\mathbf{B}$, for calculations of the objective function, the constraint values, and their sensitivity values. In order to reduce the computational cost of these calculations for a linear structure, we developed a node set selection procedure that chooses nodes whose perturbations of their displacements do not alter the stress values of the elements constructed by the nodes of the other node set. The advantages of the present procedure are that (1) it does not require direct access or modification to tailored FE software and only utilizes basic

post-processed output and (2) it can be easily extended to advanced finite element formulations such as plate and shell elements. Furthermore, localized stress-based topology optimization with advanced shell elements has not been researched in previous studies. To demonstrate the validity of the present procedure, we solved three numerical examples—an L-shaped structure, a control arm, and a wing-rib design example, and compared the obtained designs with optimized layouts produced by Altair Optistruct. Through these numerical examples, the importance of considering a three-dimensional domain for stress-based topology optimization was verified. In conclusion, we developed new numerical and optimization procedures for stress-based topology optimization within a tailored finite element code, which has previously been regarded as difficult or impossible.

Acknowledgments

This work was supported by the National Research Foundation of Korea (NRF) grant funded by the Korea government (No. 2012-0005530) and (NRF-2012R1A1A2A10038803).

References

- [1] M. Bruggi, On an alternative approach to stress constraints relaxation in topology optimization, *Struct. Multidiscip. Optim.* 36 (2008) 125–141.
- [2] G.I.N. Rozvany, Difficulties in truss topology optimization with stress, local buckling and system stability constraints, *Struct. Optim.* 11 (1996) 213–217.
- [3] R.J. Yang, C.J. Chen, Stress-based topology optimization, *Struct. Optim.* 12 (1996) 98–105.
- [4] M. Zhou, Difficulties in truss topology optimization with stress and local buckling constraints, *Struct. Optim.* 11 (1996) 134–136.
- [5] G.D. Cheng, X. Guo, Epsilon-relaxed approach in structural topology optimization, *Struct. Optim.* 13 (1997) 258–266.
- [6] P. Duysinx, M.P. Bendsoe, Topology optimization of continuum structures with local stress constraints, *Internat. J. Numer. Methods Engrg.* 43 (1998) 1453–1478.
- [7] M. Burger, R. Stainko, Phase-field relaxation of topology optimization with local stress constraints, *SIAM J. Control Optim.* 45 (2006) 1447–1466.
- [8] M. Bruggi, P. Venini, A mixed FEM approach to stress-constrained topology optimization, *Internat. J. Numer. Methods Engrg.* 73 (2008) 1693–1714.
- [9] J. Paris, F. Navarrina, I. Colominas, M. Casteleiro, Topology optimization of continuum structures with local and global stress constraints, *Struct. Multidiscip. Optim.* 39 (2009) 419–437.
- [10] C. Le, J. Norato, T. Bruns, C. Ha, D. Tortorelli, Stress-based topology optimization for continua, *Struct. Multidiscip. Optim.* 41 (2010) 605–620.
- [11] J. Paris, F. Navarrina, I. Colominas, M. Casteleiro, Block aggregation of stress constraints in topology optimization of structures, *Adv. Eng. Softw.* 41 (2010) 433–441.
- [12] Y.J. Luo, Z. Kang, Topology optimization of continuum structures with Drucker–Prager yield stress constraints, *Comput. Struct.* 90–91 (2012) 65–75.
- [13] F. van Keulen, R.T. Haftka, N.H. Kim, Review of options for structural design sensitivity analysis. Part 1: linear systems, *Comput. Methods Appl. Mech. Engrg.* 194 (2005) 3213–3243.
- [14] K.K. Choi, J.L.T. Santos, M.C. Frederick, Implementation of design sensitivity analysis with existing finite-element codes, *J. Appl. Mech., Trans. ASME* 109 (1987) 385–391.
- [15] W.H. Zhang, M. Domaszewski, H. Bassir, Developments of sizing sensitivity analysis with the ABAQUS code, *Struct. Optim.* 17 (1999) 219–225.
- [16] W.H. Zhang, M. Domaszewski, Efficient sensitivity analysis and optimization of shell structures by the ABAQUS code, *Struct. Optim.* 18 (1999) 173–182.
- [17] M. Stolpe, K. Svanberg, On the trajectories of the epsilon-relaxation approach for stress-constrained truss topology optimization, *Struct. Multidiscip. Optim.* 21 (2001) 140–151.
- [18] Q. Xia, T.L. Shi, S.Y. Liu, M.Y. Wang, A level set solution to the stress-based structural shape and topology optimization, *Comput. Struct.* 90–91 (2012) 55–64.
- [19] X. Guo, G. Cheng, K. Yamazaki, A new approach for the solution of singular optima in truss topology optimization with stress and local buckling constraints, *Struct. Multidiscip. Optim.* 22 (2001) 364–372.
- [20] G.Y. Qiu, X.S. Li, A note on the derivation of global stress constraints, *Struct. Multidiscip. Optim.* 40 (2010) 625–628.
- [21] S.H. Jeong, S.H. Park, D.H. Choi, G.H. Yoon, Topology optimization considering static failure theories for ductile and brittle materials, *Comput. Struct.* 110–111 (2012) 116–132.
- [22] T.E. Bruns, D.A. Tortorelli, Topology optimization of non-linear elastic structures and compliant mechanisms, *Comput. Methods Appl. Mech. Engrg.* 190 (2001) 3443–3459.
- [23] A.E. Inc., Altair OptiStruct 10: users manual, in, 2011.
- [24] K. Svanberg, The method of moving asymptotes—a new method for structural optimization, *Internat. J. Numer. Methods Engrg.* 24 (1987) 359–373.
- [25] M. Bruggi, P. Duysinx, Topology optimization for minimum weight with compliance and stress constraints, *Struct. Multidiscip. Optim.* 46 (2012) 369–384.